Received: 25 February 2021 | Accepted: 8 June 2021

DOI: 10.1002/vzj2.20149

Vadose Zone Journal

ORIGINAL RESEARCH ARTICLE

Investigating the controls on greenhouse gas emission in the riparian zone of a small headwater catchment using an automated monitoring system

Jihuan Wang | **Heye Bogena** | **Thomas Süß** | **Alexander Graf** | **Ansgar Weuthen** | **Nicolas Brüggemann**

Forschungszentrum Jülich, Agrosphere Institute (IBG-3), Wilhelm-Johnen-Straße, Germany D-52425

Correspondence
Jihuan Wang, Forschungszentrum Jülich, Agrosphere Institute (IBG-3), Wilhelm-Johnen-Straße, D-52425, Germany.
Email: jihuanwang.edu@gmail.com

Assigned to Associate Editor Helen Dahlke

Abstract

Riparian zones as the transition zone between terrestrial and aquatic ecosystems play an important role in C and N cycling and greenhouse gas (GHG) emissions. As such, they may help to mitigate climate change but could also accelerate it, depending on the particular processes affected by changes in the hydrologic regime. Hydrological observations indicated frequent shallow groundwater in the riparian zone, especially near the stream and during the wet winter and spring seasons with consequently frequent occurrence of soil water saturation. The redox potential was mainly governed by the soil water regime: under water saturation conditions, the redox potential of the soil decreased and returned to the oxic state after soil drainage. We found that soil temperature and soil water content were the main drivers of the variations in CO_2 fluxes, with highest CO_2 emission during summer and the lowest emissions in the winter period (162.2–5.4 mg CO_2–C m^{-2} h^{-1}). The annual average daily N_2O emission rate was low (2.3 μg N_2O-N m^{-2} h^{-1}), with the highest average daily N_2O emission in March as a result of low temperature and partial soil saturation after heavy precipitation events (37.5 μg N_2O-N m^{-2} h^{-1}). Our study showed that continuous measurement of redox potential, soil temperature, and soil water content can improve the understanding of GHG emissions in riparian zones.

1 | INTRODUCTION

Soils act as sink and source of C and N via large greenhouse gas (GHG) fluxes (Smith et al., 2007). Forest soils play an important role in controlling global warming because forests cover 31% of the global land area and are important sources of atmospheric CO_2 and N_2O (Adams, 2012; Oertel et al., 2016). Soils are also an important source and sink of N_2O and CH_4, and thus strongly influence the N_2O and CH_4 budget of the atmosphere (Chapuis-Lardy et al., 2007; Dutaur & Verchot, 2007). Oxic and anoxic zones in soils control redox reactions, including nitrification, denitrification, and the oxidation or reduction of Mn^{4+}, Fe^{3+}, and SO_4^{2-} (DeLaune & Reddy, 2005; Patrick & Jugsujinda, 1992; Reddy et al., 1989; Smith & DeLaune, 1984; Tokarz & Urban, 2015). In riparian areas, groundwater table level fluctuations cause variations of O_2 and other alternative electron acceptors

Abbreviations: Eh, redox potential; FTIR, Fourier transform infrared spectrometer; GHG, greenhouse gas; WFPS, water-filled pore space.

(e.g., NO_3^-, Mn^{4+}, Fe^{3+}, SO_4^{2-}, and CO_2), and the soil redox potential (Eh) provides a quantitative measure of oxidizing or reducing conditions in soil (Delaune & Reddy et al., 2005; Husson et al., 2016; Mansfeldt, 2003). The soil Eh range can be differentiated into oxic (>+400 mV), weakly reducing (+400 to +200 mV), moderately reducing (+200 to −100 mV), and strongly reducing (<−100 mV) conditions (Delaune & Reddy, 2005). The different oxidizing or reducing conditions govern the dynamics of CO_2, N_2O, and CH_4, and significant CH_4 production (methanogenesis) is generally active when soils are under strictly reducing conditions (Yu et al., 2008). Numerous studies investigated relationships between soil water saturation and soil Eh due to the influence of groundwater (Cogger et al., 1992; Comerford et al., 1996; Seybold et al., 2002; Thomas et al., 2009; Vepraskas & Wilding, 1983; Wanzek et al., 2018), water table changes (McDaniel et al., 2001), flooding (Brettar et al., 2002; Rinklebe et al., 2016), and irrigation (Wang et al., 2020). Redox conditions in wetland soils are strongly influenced by groundwater level fluctuations, leading to relatively fast (hourly) spatial and temporal changes of oxic and anoxic conditions and correspondingly to changes in the predominance of processes of the N cycle (i.e., ammonification and nitrification vs. denitrification) (Clément et al., 2002; Reddy et al., 1989). Furthermore, the intensity of soil redox reactions is controlled by the metabolism and biochemical transformations of microorganisms in the soil (Husson, 2013). Besides soil temperature and water content, pH, and nutrient contents (e.g. C/N ratio, NH_4^+, and NO_3^-) will influence soil biological process and cause variations of soil GHG emissions (Oertel et al., 2016). However, despite the importance of soil Eh effects, only a few studies have focused on the relationship between the soil Eh and GHG emissions in the riparian zone and found a close relationship (Marín-Muñiz et al., 2015; Phillips & Beeri, 2008; Yu et al., 2004). Soil profile analysis of soil CO_2, N_2O, and CH_4 emissions across a hydrological gradient indicated a close relationship between soil redox conditions, soil temperature, groundwater level, and potential CO_2, N_2O, and CH_4 emissions (Yu et al., 2006). Some studies reported relationships between GHG concentrations and Eh in riparian zones from water extraction or by measuring only the surface layer (0–5 cm) (Marín-Muñiz et al., 2015; Poblador et al., 2017). However, these studies failed to obtain a full picture of the controlling factors of biogeochemical processes in riparian zones, and important influencing factors on GHG emissions were not analyzed in detail at the different depths with high time resolution, such as soil Eh or matrix potential, which are essential for estimating soil GHG emissions more accurately and for improving the current estimates or models.

In this paper, we present a newly developed automated soil Eh measurement system, in which the variations in GHG (CO_2, CH_4, and N_2O) emissions along with other important soil variables (soil water content, soil temperature, soil matrix potential, and groundwater table level) can be simultaneously observed. We deployed this monitoring system in the riparian zone of the Wüstebach catchment, Germany, and conducted continuous measurements over 1 yr. The obtained dataset was used to investigate the abovementioned control parameters and their effect on GHG emissions in the riparian zone.

Core Ideas

- An automated measurement system was used to capture the soil hydrological parameters and Eh.
- Eh showed significant spatiotemporal variations due to the hydrological gradients and events.
- Soil Eh was slightly positively correlated with CO_2.
- Monthly average CO_2 emissions show a negative linear relationship with groundwater table depth.
- The average Eh at −30 cm has a quadratic relationship with the distance to the stream.

The main objectives of this study were (a) to establish continuous subdaily soil Eh and soil CO_2, N_2O, and CH_4 flux measurements in a riparian zone; (b) to identify if the variations of soil Eh influenced by slope and water table fluctuations in different distances from the stream, and (c) to study the relationships between GHG fluxes and environmental factors.

2 | MATERIALS AND METHODS

2.1 | Site description and instrumentation

The study was carried out in the TERENO test site Wüstebach (50°34′ N, 6°25′ E), a headwater catchment covering an area of 38.5 ha (Figure 1; Bogena et al., 2018). The catchment is located in the German low mountain range near the German–Belgian border and belongs to the Eifel National Park. Elevation ranges from 595 to 628 m asl with an average slope of 3.6% (Bogena et al., 2018). The catchment is located in the humid temperate climatic zone with a mean annual precipitation of 1,200 mm and a mean annual temperature of 7 °C (Wiekenkamp et al., 2016). The bedrock consists of Devonian shales with sporadic sandstone inclusions and is covered by a 1-to-2-m-thick periglacial solifluction layer in which mainly Cambisols in the western part and stagnic Cambisols in the eastern part have developed in the groundwater distant hillslopes. In the valleys, groundwater has a considerable influence, and here Planosols are associated with Gleysols and semi bogs (Histosols) (Bogena et al., 2018). The soil texture is silty clay loam with medium to very high fraction of coarse material. Prior to the forest redevelopment, the

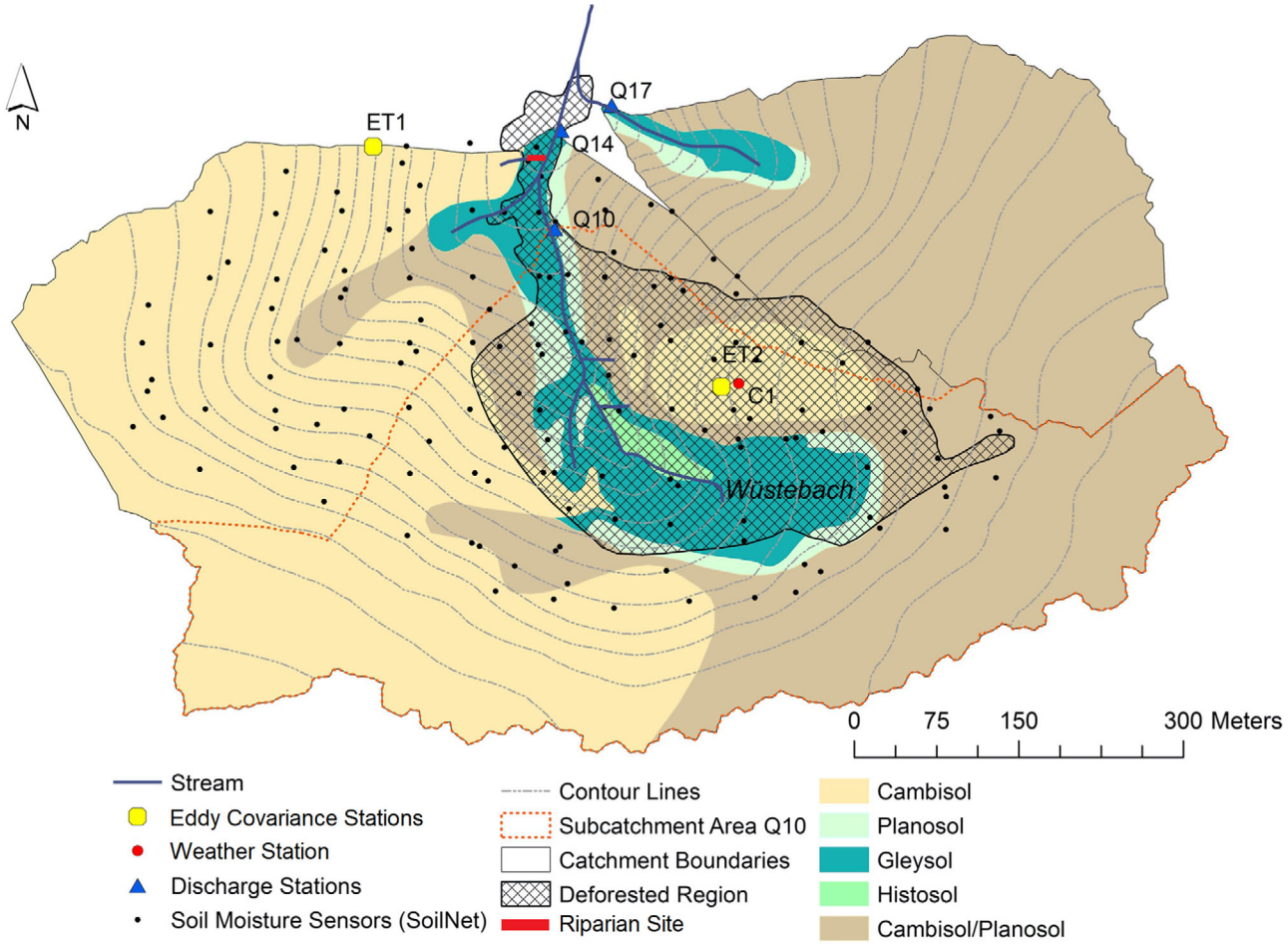

FIGURE 1 Map of the Wüstebach catchment including the riparian site and the weather station (Wiekenkamp et al., 2016, modified)

catchment area was almost completely covered by Norway spruce (*Picea abies* L.) and Sitka spruce [*Picea sitchensis* (Bong.) Carr.], which were planted in the late 1940s with an average density of 370 trees ha^{-1}. In August 2013, a partial deforestation took place in the catchment area of the Wüstebach, whereby all spruce trees in the riparian zone and its immediate surroundings were removed using a cut-to-length method (Figure 1).

2.2 | Experimental setup

The experimental setup was installed in the deforested riparian zone (Figure 1) and consisted of five soil stations combined with automated soil chambers for GHG flux measurements, which were set up along a transect perpendicular to the stream (Figure 2). The soil stations were installed on 19 and 20 July 2018 and were equipped with multiple soil sensors in three depths (Figure 2b). The measurement period lasted from October 2018 to September 2019. The soil GHG collection system was installed in October 2018. All soil sensors had been installed previously and had been allowed to equilibrate in situ 2 mo prior to the start of data collection. Due to the varying depth and high stone content of the subsoil, it was not possible to select exactly the same depths for the medium and deep sensor levels. In order to be able to capture short-term changes in GHG emission rates during hydrological events (e.g., soil redox conditions can change within hours after rainfall due to soil saturation or groundwater rise and promoting the emission of CH_4 or N_2O), soil Eh measurements were performed with high time resolution, which is a prerequisite for the detailed analysis of the controls of Eh on GHG emissions. All measurement data (except GHG flux data) were recorded continuously every 15 min and transmitted using the recently developed wireless sensor network SoilNetLoRa (Forschungszentrum Jülich), which is based on the sub-gigahertz LoRa technology (Bogena, 2019). Data were transmitted and uploaded in near-real time to a network server, where they were retrieved by an application software. Meteorological data were taken from the TERENO climate station WU_EC_002 (50°50′ N, 6°33′ E), also located in the deforested area of the Wüstebach catchment (Figure 1). Below, the automated soil and GHG emission monitoring system is described in detail.

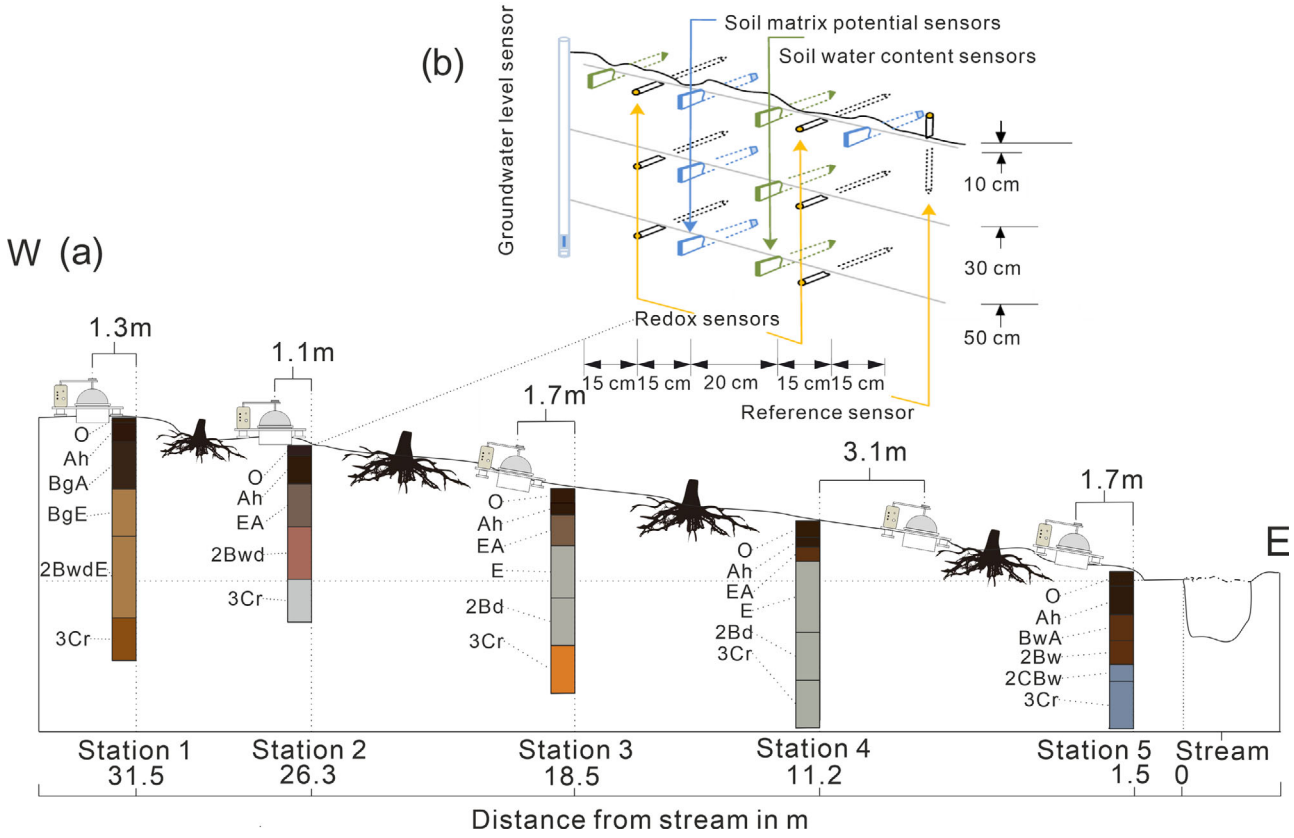

FIGURE 2 (a) Locations of the soil profiles and chambers along the experimental transect in the riparian zone of the Wüstebach catchment. Individual soil layers are indicated by different colors, and letters indicate horizon names based on USDA classification (see Table 1). (b) Schematic depicting the soil monitoring system consisting of four soil moisture sensors, four matrix potential sensors, six redox potential sensors, and one groundwater level sensor

Redox potential was measured using a system of several platinum electrodes and one reference electrodes (Type 4621, Ecotech) with a resolution of 0.1 ± 3 mV. This soil Eh measurement system was first developed by Mansfeldt (2004). Six platinum electrodes were installed ~10, ~30 and ~50 cm below the soil surface, and a reference electrode with Ag/AgCl salt bridge (Ecotech) was inserted next (within 45 cm) to the soil profile (Mansfeldt, 2003). The KCl gel of the reference electrodes were refilled every 2–4 wk (depending on soil dryness) to ensure good contact between soil and redox electrode. The Eh measurements were related to the normal hydrogen electrode using the following equation:

$$\mathrm{Eh} = E + E_{\mathrm{ref}} \quad (1)$$

in which E is the potential measured against the Ag/AgCl reference electrode, and E_{ref} is the voltage difference between the standard hydrogen reference electrode and the Ag/AgCl reference electrode (+210.5 mV at 20 °C). The E values were corrected by adding a correction value, relating them to the standard hydrogen electrodes according to the temperature and pH value in different layer. The pH values of the different soil layers were between 3.3 and 3.9 (Table 1). A predicted change in Eh of −59 mV occurs if the pH changes by one unit. Therefore, Eh is commonly referenced to pH 7 to make Eh values in different soils comparable (Bohn, 1971; Fiedler et al., 2007).

Soil water content and matrix potential were measured using SMT100 sensors (Truebner) and TensioMark sensors (Ecotech), respectively. Although two redox sensors were installed in parallel at each depth, SMT100 and TensioMark sensors were only doubled in the first layer (Figure 2) because the surface soil and its stronger variations of soil microbial activity has a higher impact on the surface gas emissions. The SMT100 soil water content sensor uses a ring oscillator with a steep pulse and oscillation frequencies between 150 and 300 MHz (Bogena et al., 2017) and also measures soil temperature using a digital temperature sensor (ADT7410, Analog Devices) with an accuracy of ± 0.4 °C. The TensioMark sensor determines the matric potential from 1 to 10^7 hPa by measuring the water content of a porous ceramic with known water retention characteristics using heat dissipation (Durner & Or, 2006). Soil water-filled pore space (WFPS) values were

TABLE 1 Soil properties of the five soil profiles

Profile	USDA horizon	Depth	pH ($CaCl_2$)	TOC	Total N	Bulk density	Total pore volume
		cm		——%——		g cm^{-3}	%
1	O	2–0	3.3	–	–	–	–
	Ah	0–8	3.5	10.50	0.61	0.5	–
	BgA	8–28	3.8	5.20	0.35	0.8	84.0
	BgE	28–48	4.0	0.94	0.12	1.4	73.2
	2BwdE	48–82	4.0	0.38	0.09	1.6	52.9
	3Cr	82+	4.0	0.38	0.07	n.d.	46.4
2	O	4–0	3.3	–	–	–	–
	Ah	0–12	3.3	12.20	0.62	0.6	77.9
	EA	12–30	3.9	9.30	0.53	0.7	75.8
	2Bwd	30–52	4.0	0.45	0.08	1.4	49.2
	3Cr	52–75	–	–	–	–	–
3	O	6–0	3.7	–	–	–	–
	Ah	0–5	3.6	15.40	–	0.4	88.3
	EA	5–18	3.7	–	–	0.8	86.0
	E	18–40	4.0	–	–	1.2	59.3
	2Bd	40–60	4.1	–	–	–	–
	3Cr	60–80	4.2	–	–	–	–
4	O	7–0	–	–	–	–	–
	Ah	0–4	3.6	15.40	–	0.4	–
	EA	4–10	3.7	–	–	0.8	88.3
	E	10–40	4.0	–	–	1.2	86.0
	2Bd	40–60	4.1	–	–	–	59.3
	3Cr	60–80	4.2	–	–	–	–
5	O	6–0	–	–	–	–	–
	Ah	0–12	3.5	15.40	>1.20	0.4	81.3
	BwA	12–23	3.5	16.90	1.20	1.3	82.1
	2Bw	23–33	3.9	12.50	0.96	–	–
	2CBw	33–40	3.9	–	–	–	–
	3Cr	40–70	4.0	–	–	–	–

derived from the soil water content measurements according to the following equation:

$$\mathrm{WFPS} = \frac{\mathrm{SWC}}{1 - \frac{\mathrm{BD}}{2.65}} \quad (2)$$

where WFPS is the water-filled pore space value (%), SWC is the soil water content (vol.%), BD is the soil bulk density (g cm^{-3}), and 2.65 is the typical density of soil minerals (g cm^{-3}).

Groundwater level was monitored at each of the five locations using CTD-10 sensors (METER Group) installed in groundwater wells. The CTD-10 sensor uses a vented differential pressure transducer to measure the pressure from the water column to determine water depth with a resolution of 2 mm. The depths of groundwater wells ranged between 57.8 and 73.5 cm, depending on soil thickness. The trends in the Eh data at the beginning of the measurement period indicate that an equilibration period of 2–3 wk is needed after installation before the sensors provide reliable measurements (e.g., due to contact issues). At Station 3, a longer data gap occurred from 10 to 28 Aug. 2018 because the agar gel of the reference electrode shrank, and the electrode lost contact with the soil due to the dry soil conditions. Thus, it is important to check the agar gel condition on a weekly basis during the summer months and the reference electrode needs to be refilled with new agar gel if needed. However, because the Eh sensors were not yet in equilibrium and the failure of sensors and power supply often occurred during the period, we did not use the data from this period.

Greenhouse gas emissions were determined at each of the five stations with automated opaque long-term chambers (8100-104, LI-COR Biosciences) as depicted in Figure 2. The height of the chamber was 33 cm, and the chamber covered a soil area of 317.8 cmš and has a volume of 4,076 cmş. The atmosphere of the chambers was circulated via the LI-8150 multiplexer (LI-COR Biosciences) to the central infrared CO_2 gas analyzer (LI-8100A, LI-COR Biosciences). A Fourier transform infrared spectrometer (DX4015 FTIR analyzer, Gasmet Technologies) was used to measure CO_2, CH_4, and N_2O concentrations. The FTIR analyzer was passively integrated in the flow system, using the pump of the LI-8100A and the multiplexer. After FTIR analysis, the gas flowed back to the multiplexer and from there to the corresponding chamber, resulting in a closed-loop system. The maximal flow rate of the loop system was 1.7 L min^{-1}. Due to the flow-through setup, the effective chamber volume used for the GHG flux calculation consisted of the total volume of the measurement loop (5,868.7 cmş for Stations 1 and 2, and 5,631.7 cmş for the remaining stations).

The closure time of the chambers was set to 5 min at the beginning of the experiment, resulting in 24 measurements per day. On 15 Jan. 2019, the closure time was set to 15 min to allow more stable GHG flow measurements, resulting in eight measurements per day (3-h frequency). In contrast, the FTIR analyzer continuously measured with an interval of 20 s. Therefore, the data had to be merged during the data post-processing. The automatic GHG flux measurement system and data post-processing compared the CO_2 fluxes measurements from the FTIR and Li-Cor system; when the results are similar and the start CO_2 concentration was below 1,000 µmol mol^{-1}, the fluxes results of N_2O are accepted (Supplemental Figure S1). Subsequently, the processed chamber headspace GHG concentrations were used to calculate CO_2, CH_4, and N_2O fluxes from linear regression functions (Brümmer et al., 2008; Collier et al., 2014; Parkin & Venterea, 2010; Wang et al., 2018; Wagner, 2019):

$$F = \frac{\Delta c}{\Delta t} \cdot \frac{10^6}{10^9} \cdot \frac{60 \cdot V_{Ch} MW}{A_{Ch} MV_{Corr}} \quad (3)$$

where F is the flux (in mg m^{-2} h^{-1} or µg m^{-2} h^{-1}), and $\Delta c/\Delta t$ is the slope of the linear regression (in µmol mol^{-1} min^{-1} or nmol mol^{-1} min^{-1}). A_{Ch} (m^{-2}) and V_{Ch} (m^{-3}) are the base area and volume of the Li-COR chamber, respectively. MV_{Corr} is the pressure- and temperature-corrected molar volume of air (m^{-3} mol^{-1}), with $MV_{Corr} = 0.02241 \cdot [(273.15 + t)/273.15)]/(p_0/p_1)$, where t is the chamber headspace air temperature during the measurement (°C), p_0 is the standard atmospheric air pressure (Pa), and p_1 is the air pressure during the measurements (Pa). MW is the molecular weight of CO_2–C, CH_4–C, or N_2O-N. Snow on the soil surface was removed during periods of snowfall. Due to occasional instrument failure of the GHG collecting system, in situ soil gas emission measurements were not continuously available at our sites. Therefore, GHG data with at least one valid CH_4 and CO_2 flux measurement per day are only available for 283 d, and for N_2O only for 269 d.

2.3 | Soil sampling and laboratory analysis

The soil horizons of the five soil profiles were sampled on 18 and 19 June 2018. The soil properties of the five soil stations are summarized in Table 1. Additionally, soil samples were collected on 20 Dec. 2018 for soil NH_4^+ and NO_3^- concentration analysis. Theses samples (three replicates) were taken from 0–30 cm using a HUMAX SH 300 soil sampler (Humax Soil Sampling Technologies) at five points near the automated soil chambers. After collection, the samples were divided into three different depths (0–10, 10–20, and 20–30 cm), sieved to 2 mm and then extracted with 50 ml 0.1 M $CaCl_2$ solution. The extract was then analyzed for inorganic N concentrations (NH_4^+ and NO_3^-) using a Dionex ICS-3000 ion chromatography system.

2.4 | Statistical analysis

We performed regression analyses and explored the relationships between WFPS, soil temperature, and GHG fluxes linear mixed-model ANOVA to test for significant differences. Multiple linear and nonlinear regression analyses were performed with the corresponding R packages to evaluate the influence of soil temperature and soil water content and to obtain a simple model of GHG emission rates. The calculation of the annual CO_2 emission rate was based on daily average values, and a linear interpolation between adjacent values was applied to fill the periods when data were missing.

3 | RESULTS

3.1 | Meteorology and soil data

The highest and lowest monthly rainfall during the observation period (October 2018–October 2019) occurred in December (205 mm) and July (38 mm), respectively (Figure 3). Total precipitation was 1,079 mm, below the average annual precipitation of 1,220 mm (Bogena et al., 2018). Monthly air temperature ranged between −1.4 and 16.7 °C, and soil temperature ranged between 2.7 and 14.9 °C. Figure 4 presents the concentrations of soil NO_3^- and NH_4^+ at the five measurements stations for three different soil layers (0–10, 10–20, and 20–30 cm). At almost all stations, NH_4^+ and NO_3^- concentrations in the soil decreased with depth (Figures 4a and 4b).

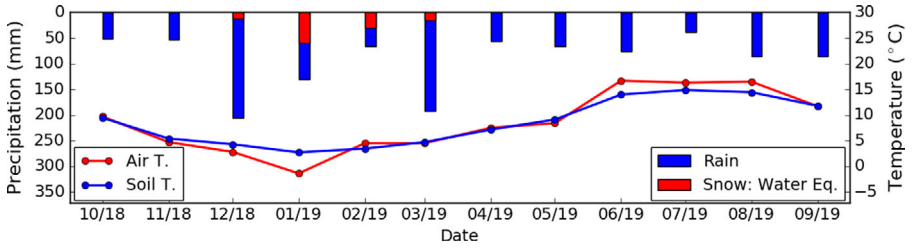

FIGURE 3 Monthly precipitation and temperature (T) data during the observation period

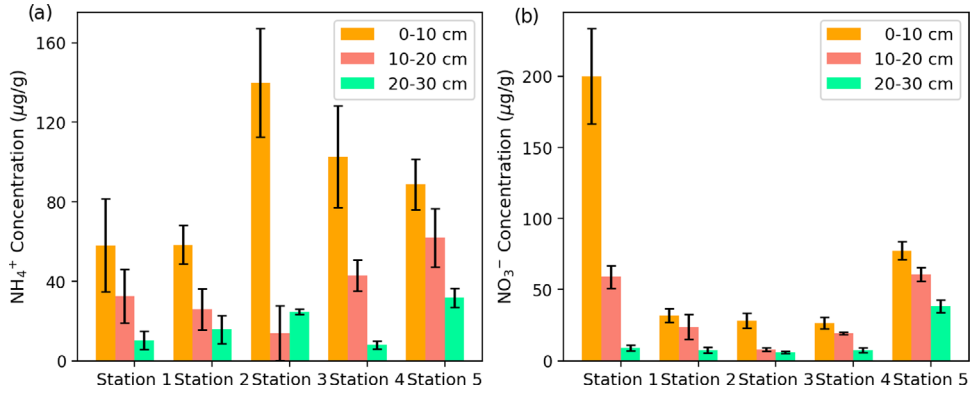

FIGURE 4 Soil (a) NH_4^+ and (b) NO_3^- concentration in the three different soil layers (from 0–10, 10–20, and 20–30 cm) from the soil sampling on 20 Dec. 2018 and the error bars represent the standard deviations

The mean NH_4^+ concentrations of the first layer down to the third layer were 89.5, 35.4, and 18.1 μg g^{-1}, respectively, whereas the corresponding mean NO_3^- concentrations were 72.8, 34.2, and 13.7 μg g^{-1}, respectively.

3.2 | Variations in soil hydrological state variables and soil Eh

Compared with summer, the relatively high amounts of precipitation and low evapotranspiration rates during the winter and spring months resulted in a generally shallow groundwater table with correspondingly high soil water contents and soil matrix potentials close to 0 mbar (Figure 5). The high soil wetness reduced the exchange of air between atmosphere and soil, which led to a decline in the average soil Eh at all depths until a rainless period in June 2019 occurred and the soil started to dry out, as indicated by a significant decrease in matrix potential (Figure 5). The groundwater level and the matrix potential were generally higher at the two stations closest to the stream (Stations 4 and 5, Supplemental Figures S5 and S6), indicating a hydrological gradient within the riparian zone. During June 2019, Eh at both −10- and −30-cm depth increased from below +400 mV to values above +600 mV within 15 d, indicating oxic conditions due to better air exchange with the atmosphere (Figure 6). After June 2019, the soil Eh values at 50-cm depth remained largely at a low level (<+200 mV) at Stations 3, 4, and 5. The WFPS (46–100%) and soil Eh (−292 to +656 mV) in the five stations exhibited large variability across the riparian zone (Table 2 and Supplemental Figures S2–S6). From Supplemental Table S1, the correlation values (Pearson's r) between Eh and groundwater table level were between .70 and .74, and between SWC and groundwater table they ranged from −.93 to −.91. The soil Eh was below 400 mV during winter and spring, and most of soil under oxic conditions after June 2019, with the soil Eh at −30 cm increased to values above +400 mV. Surprisingly, the lowest Eh values were recorded at −10 cm (−257 mV) at Station 4 after a long period of water saturation, which was even more than 100 mV lower than the minimum redox value at the other stations (1, 2, 3, and 5). When the groundwater table level was above the electrode at −10 cm after strong rainfall events during the rainy period, Eh at −10 cm at Stations 2 and 3 dropped by 200 mV or more. At Stations 4 and 5, both redox sensors installed at −50 cm were fully immersed in the groundwater during most of the monitoring period (Supplemental Figures S5 and S6). Accordingly, the Eh values deviated only slightly from the mean value of this depth (−73 ± 68 mV and 50 ± 83 mV respectively), and indicated reducing conditions in this layer (Table 2). On the other hand, the redox sensors installed at −10- and −30-cm depths as Stations 3, 4, and 5 showed considerably higher Eh

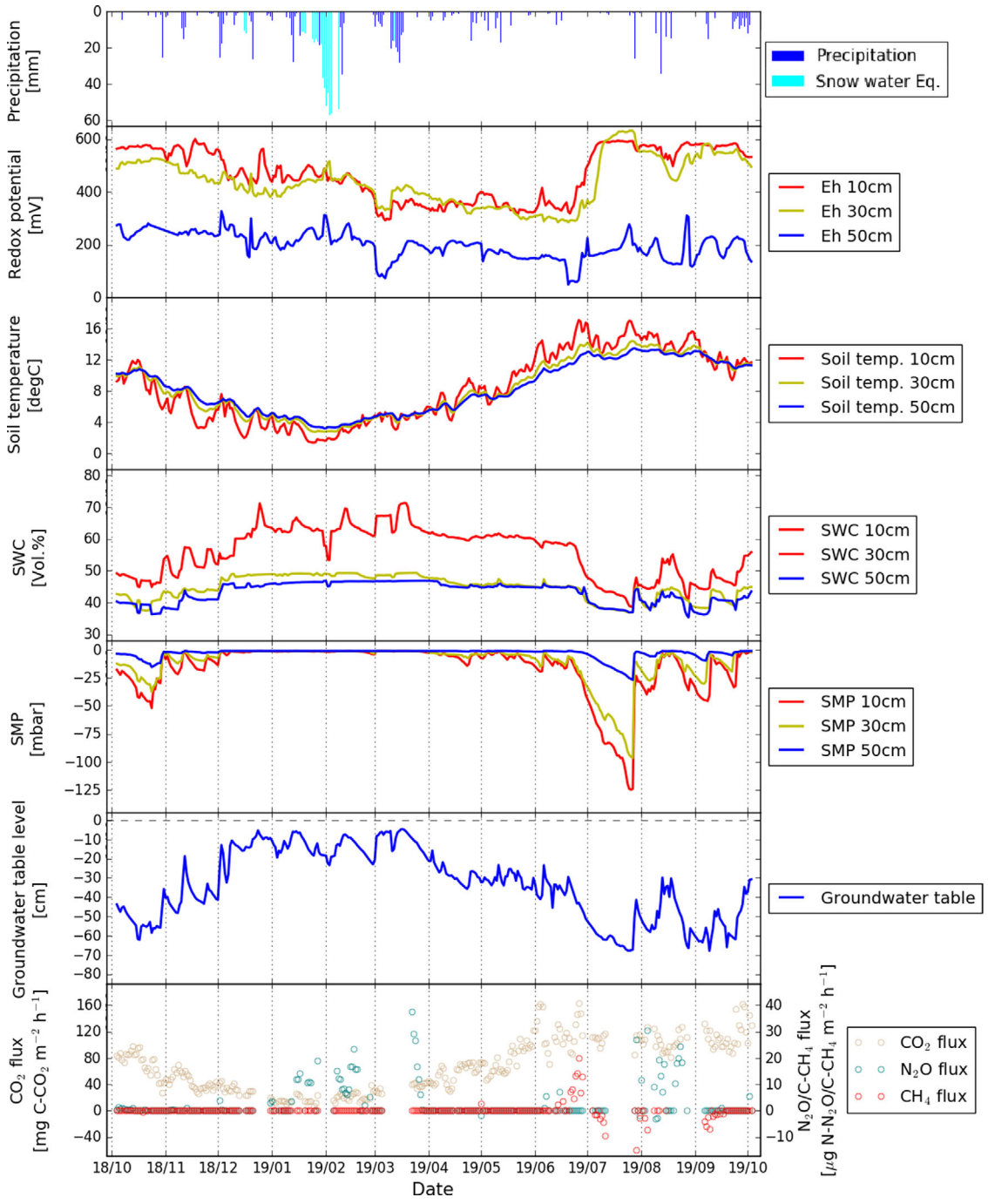

FIGURE 5 Time series of daily sums of precipitation, snow cover, and daily means of redox potential (Eh), soil temperature (temp.), SWC (volumetric soil water content), SMP (soil matrix potential), groundwater table depth, and greenhouse gas fluxes at all five stations

and larger SD values (Table 2). Figure 7 shows daily average Eh at the different depths and the relations with the distance to the stream. The distance to the stream had a quadric relation with Eh at −30 cm ($R^2 = .99, p < .001$), whereas it had a linear relationship with the Eh at −50 cm ($R^2 = .80, p = .04$). Except at Station 5, the soil Eh values at −30 and −50 cm were positively correlated with the distance to the stream. Moreover, Supplemental Figure S7 shows a negative linear relationship between Eh at −10 cm and groundwater table level on a daily scale. This relation showed hysteretic behavior: the green and red dots indicate the soil rewetting phase, while the blue dots indicate the soil drying phase.

3.3 | Variations in GHG emissions

All daily mean CO_2 fluxes were greater than zero and valid (nonzero), whereas N_2O and CH_4 fluxes were significantly

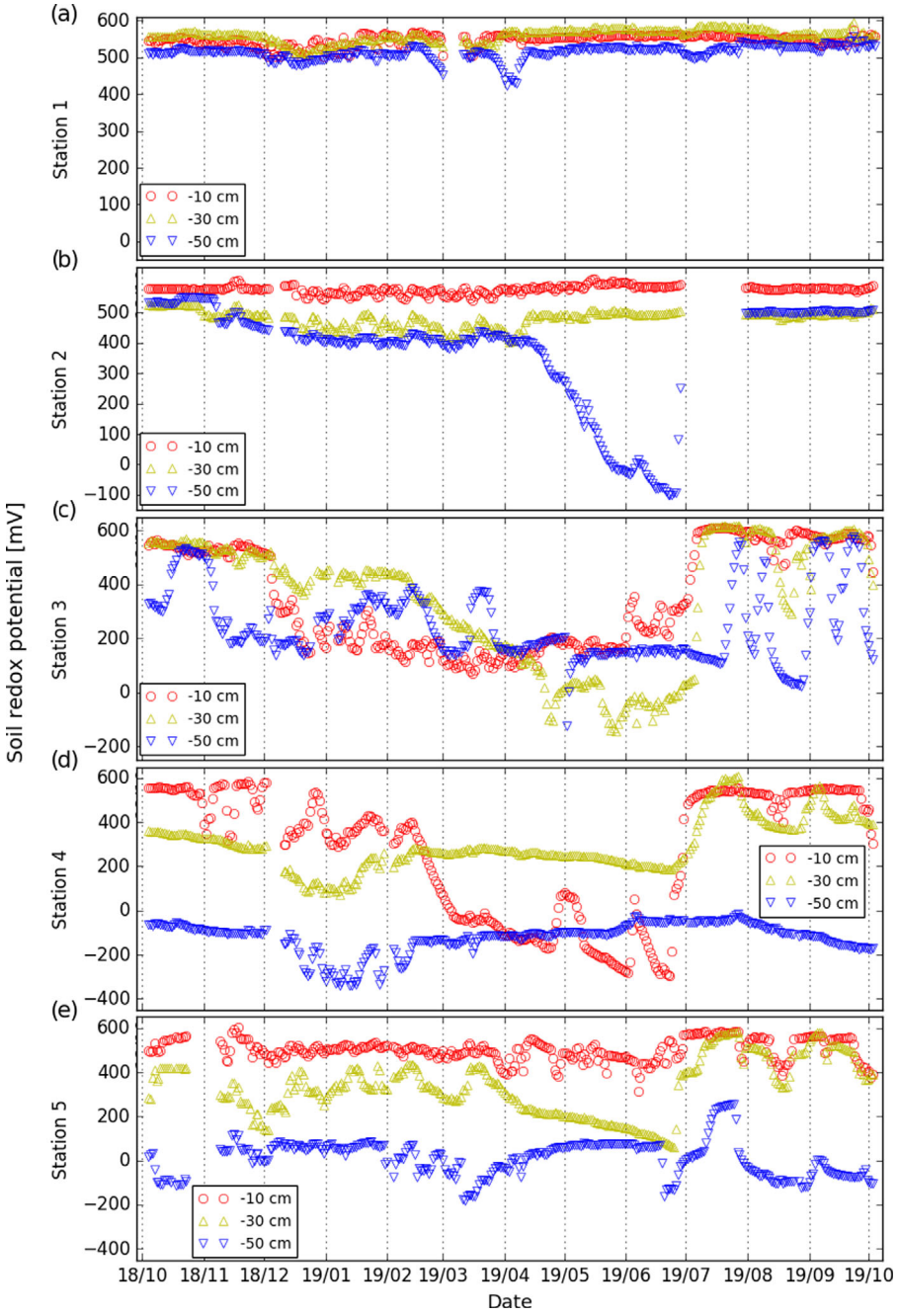

FIGURE 6 Daily redox potential at different depths at the five stations

different from zero on only 73 and 32 d, respectively. The soil CO_2 emissions ranged from 54.00 ± 33.50 to 103.96 ± 61.73 mg C m^{-2} h^{-1} between Station 1 and Station 5. They tended to be lowest during the winter season, whereas the highest CO_2 emission rates were observed in June simultaneously with the lowest soil water content and the highest soil temperature (Figure 5). The CO_2 flux varied significantly between the stations ($p < .01$). The highest and lowest mean daily CO_2 flux rates were measured at Stations 2 and 4 with 270.03 and 7.09 mg C m^{-2} h^{-1}, respectively. The annual average soil CO_2 emission rate across all stations was 71.58 ± 44.73 mg C m^{-2} h^{-1} (Table 3). The coefficient of variation for CO_2 fluxes at Station 1 was 35.5% (Table 3), whereas it was between 55 and 63% at the other stations.

The seasonal variations of N_2O emissions were less pronounced than for CO_2, and on most of the measurements (1177/1250, 94%), we found no N_2O emissions significantly different from zero (absolute flux value < 5 μg N m^{-2} h^{-1}). The lowest mean annual N_2O emission (0.37 ± 3.51 μg N m^{-2} h^{-1}) was found at Station 1 (Table 3), which was 16% of the mean annual N_2O emission rate of all the stations (2.26 ± 12.72 μg N m^{-2} h^{-1}), and the uptake of N_2O was observed at Station 5 (−0.34 ± 4.12 μg N m^{-2} h^{-1}) (Table 3). A significant short-term increase of the N_2O

TABLE 2 Statistics of redox potential (Eh) measurements at the five stations in the three different depths

Station	Depth	Mean Eh	Min, Eh	Max. Eh	Range	CV	Redox status[a]
	cm	mV				%	
Station 1	10	565 ± 14[b]	520	591	71	2.5	I
	30	596 ± 15	545	628	83	2.6	I
	50	554 ± 17	466	597	130	3.1	I
Station 2	10	578 ± 11	544	611	67	1.9	I
	30	483 ± 26	405	528	122	5.4	I
	50	417 ± 174	−60	592	652	41.8	I
Station 3	10	372 ± 189	96	630	533	50.8	II
	30	384 ± 230	−104	656	760	59.9	II
	50	293 ± 135	−75	624	700	46.1	II
Station 4	10	316 ± 291	−257	631	888	92.0	II
	30	342 ± 113	117	645	527	32.9	II
	50	−73 ± 68	−292	28	321	−93.1	III
Station 5	10	513 ± 49	321	621	300	9.5	I
	30	377 ± 128	99	621	521	34.0	II
	50	50 ± 83	−136	293	429	165.0	III

[a]Redox status: I, oxidizing (>+400 mV); II, weekly reducing (+400 to +200 mV); III, moderately reducing (+200 to −100 mV); IV, strongly reducing (<−100 mV) (Mansfeldt et al., 2003).
[b]Standard deviation.

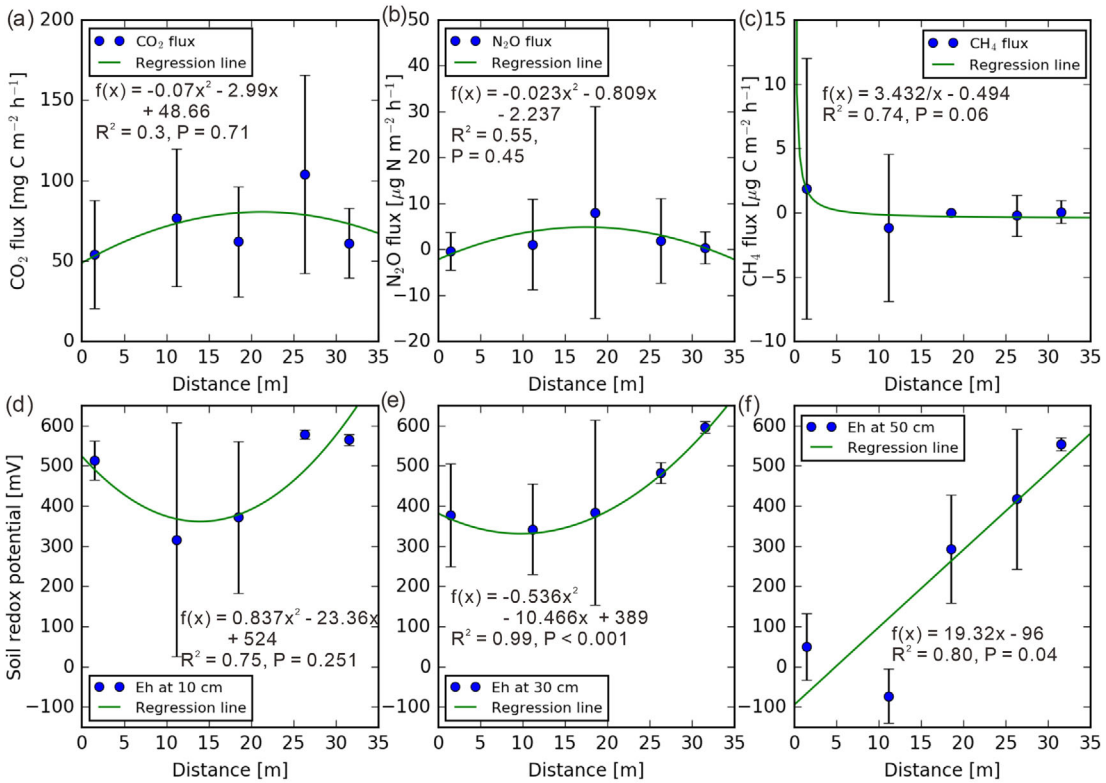

FIGURE 7 Greenhouse gas fluxes, soil redox potential (Eh), and the different distances from the stream

TABLE 3 Mean annual and maximum and minimum mean daily fluxes of CO_2, N_2O, and CH_4 with the coefficient of variation at Wüstebach

Flux	Station 1	Station 2	Station 3	Station 4	Station 5	Mean, Stations 1–5
CO_2, mg C m^{-2} h^{-1}						
Annual mean (± SD)	61.09 ± 21.74	103.96 ± 61.73	62.05 ± 34.32	76.78 ± 42.75	54.00 ± 33.50	71.58 ± 44.73
Max.	113.35	270.03	156.29	227.29	134.28	270.03
Min.	23.04	9.17	7.10	7.09	7.14	7.09
N[a]	231	244	257	267	251	1250
CV, %	35.59	59.39	55.31	55.68	62.04	62.49
N_2O, µg N m^{-2} h^{-1}						
Annual mean (± SD)	0.37 ± 3.51	1.93 ± 9.27	8.03 ± 23.05	1.09 ± 9.89	−0.34 ± 4.12	2.26 ± 12.72
Max.	43.36	89.28	152.97	122.60	9.18	152.97
Min.	−8.97	−15.70	−9.97	0	−46.93	−46.93
N	231	244	257	267	251	1250
CV, %	962.44	482.00	287.29	911.52	−1,193.47	563.99
CH_4, µg C m^{-2} h^{-1}						
Annual mean (± SD)	0.06 ± 0.90	−0.22 ± 1.60	0 ± 0	−1.16 ± 5.73	1.88 ± 10.12	0.10 ± 5.40
Max.	13.30	0	0	0	79.89	79.89
Min.	0	−15.18	0	−59.12	0	−59.12
N	215	230	241	253	236	1175
CV, %	1,466.29	−711.83	0	−494.78	538.66	5,660.81

[a]*N*, number of valid CO_2, N_2O, and CH_4 fluxes.

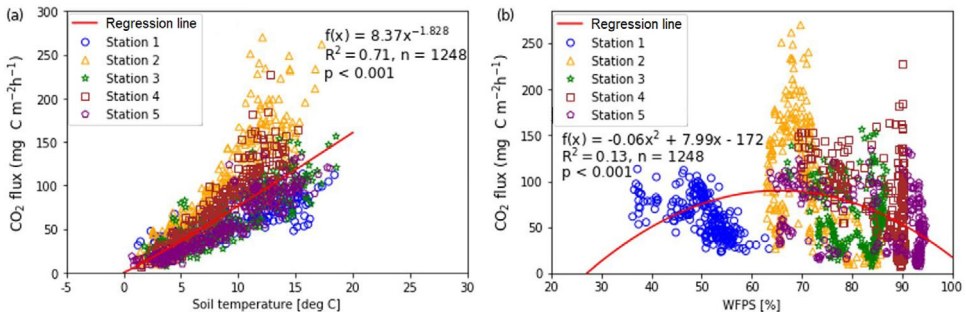

FIGURE 8 Relationship between daily CO_2 fluxes and (a) soil temperature and (b) WFPS (soil water-filled pore space)

emission in winter was observed for Stations 2 and 3. The annual daily mean CH_4 fluxes fluctuated between the stations from −59.12 to 79.89 µg C m^{-2} h^{-1}. Substantial CH_4 emission was found at the near-stream Station 5, whereas at Station 4, negative CH_4 fluxes were observed indicating net CH_4 uptake (Table 3). However, for most of the measurements (1142/1175, 97%), CH_4 fluxes were zero or close to zero (absolute flux value < 5 µg C m^{-2} h^{-1}).

3.4 | Correlation of CO_2 fluxes with environmental variables

Both soil temperature and WFPS played a vital role in governing CO_2 fluxes in our study. The CO_2 flux correlated significantly with soil temperature at −10 cm and water table depth (with a Pearson's correlation coefficient of .93 and .61, respectively) (Supplemental Table S1). A simple exponential model was used to describe the temperature dependency of the soil CO_2 fluxes, using soil temperature measurements at 10-cm depth (R^2 = .71, p < .001) (Figure 8a). In contrast, a quadratic relationship of CO_2 fluxes with WFPS was found, but with much lower R^2 (R^2 = .13, p < .001) (Figure 8b). The lowest CO_2 emission was found at Station 5 (54 ± 33.5 mg C m^{-2} h^{-1}), whereas CO_2 emission rates where significantly higher for the other stations (61.09 ± 21.74 to 103.96 ± 61.73 mg C m^{-2} h^{-1}). Also a significant, albeit weaker, relationship between daily CO_2 flux and daily soil Eh was found (Pearson's r = .20∼.22) (Supplemental Table S1).

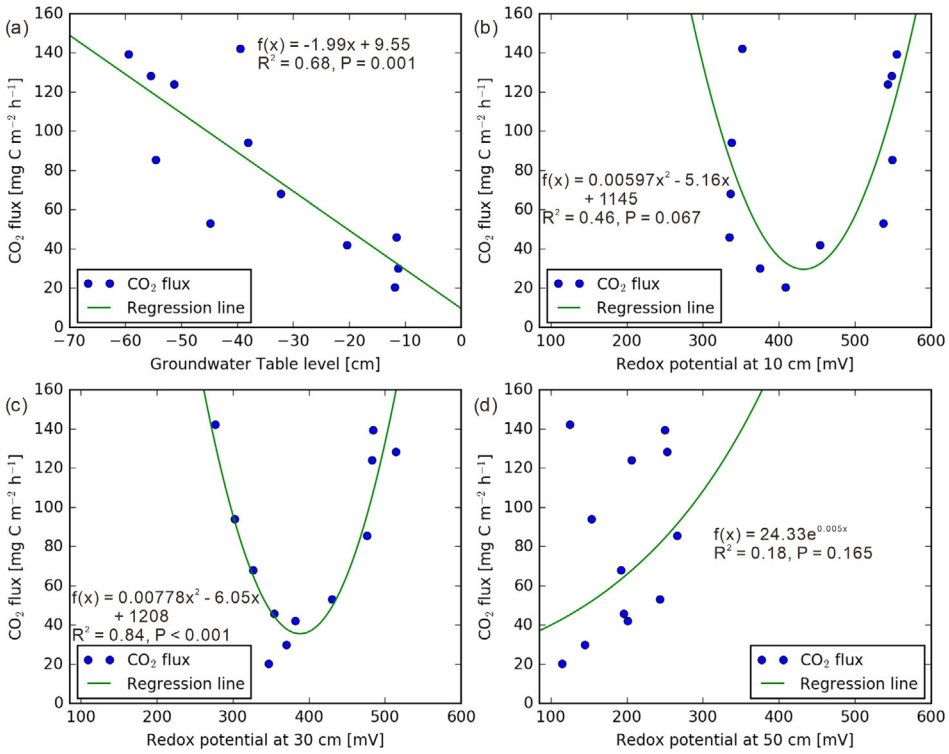

FIGURE 9 Correlations between monthly means of CO_2 fluxes and groundwater table level, and with soil redox potential (Eh) at different depths (mean of all stations)

Figure 9a shows the linear regression between the monthly mean CO_2 fluxes and the groundwater table depths ($R^2 = .68$, $p = .001$). Furthermore, Figures 9b and 9c show the quadratic relationship between monthly average CO_2 flux and Eh at −10 and −30 cm. The minimum CO_2 flux values of the functions occurred when soil Eh values were +389 and +433 mV, respectively (i.e., close to +400 mV, which is the value that separates the Eh into oxic and weakly reducing conditions).

3.5 | Correlation of N_2O fluxes and CH_4 fluxes with environmental variables

During the periods of high groundwater table in winter, N_2O emission events occurred at all five stations, with the main emission events occurring at Stations 2 and 3 (Figure 10b). Most of the N_2O emissions events at Station 3 occurred when the soil Eh value at −10 cm was below +400 mV and between +100 and +200 mV. The correlations between the N_2O flux and the other soil variables were mostly weak (Supplemental Table S1). The CH_4 emission rates during our experiment were rare. From Figure 10c, it becomes apparent that only Station 5 showed notable CH_4 emissions between 18 and 28 June 2019, with a total CH_4 emission of 11.6 mg C m^{-2} (calculated from the daily average emission rates). The CH_4 emission events started after soil Eh at −50 cm decreased to values below −100 mV as the result of stronger rainfall events during summer 2019 (Figures 6e and 9c). The CH_4 emission coincided with low soil Eh values (+200 mV) at −30 cm that are suitable for CH_4 to pass through this soil layer without being oxidized (Supplemental Figure S6). However, Station 3 showed no significant CH_4 emissions, even though the Eh at −30 cm had a similarly low soil Eh (−89 ± 13 mV) from May 24 to 28, 2019. In contrast, several CH_4 uptake events occurred at Station 4 in July and August at soil Eh values above +400 mV at −10 and −30 cm and around 0 mV at −50 cm. The significant CH_4 uptake events at Station 4 occurred when the daily average soil Eh was above +350 mV, and large quantities of CH_4 were produced after the Eh fell below a critical threshold of +200 mV at Station 5 (Supplemental Figure S8).

3.6 | Multivariate regression analysis

Below, a linear stepwise regression analysis was used to find environmental variables (soil temperature, water-filled pore space, soil matrix potential, and soil Eh) that can predict the measured soil GHG fluxes. It has to be noted that analyzed environmental variables were not completely independent and could change with depth (Supplemental Table S2). In the model, the soil GHG fluxes are considered as dependent

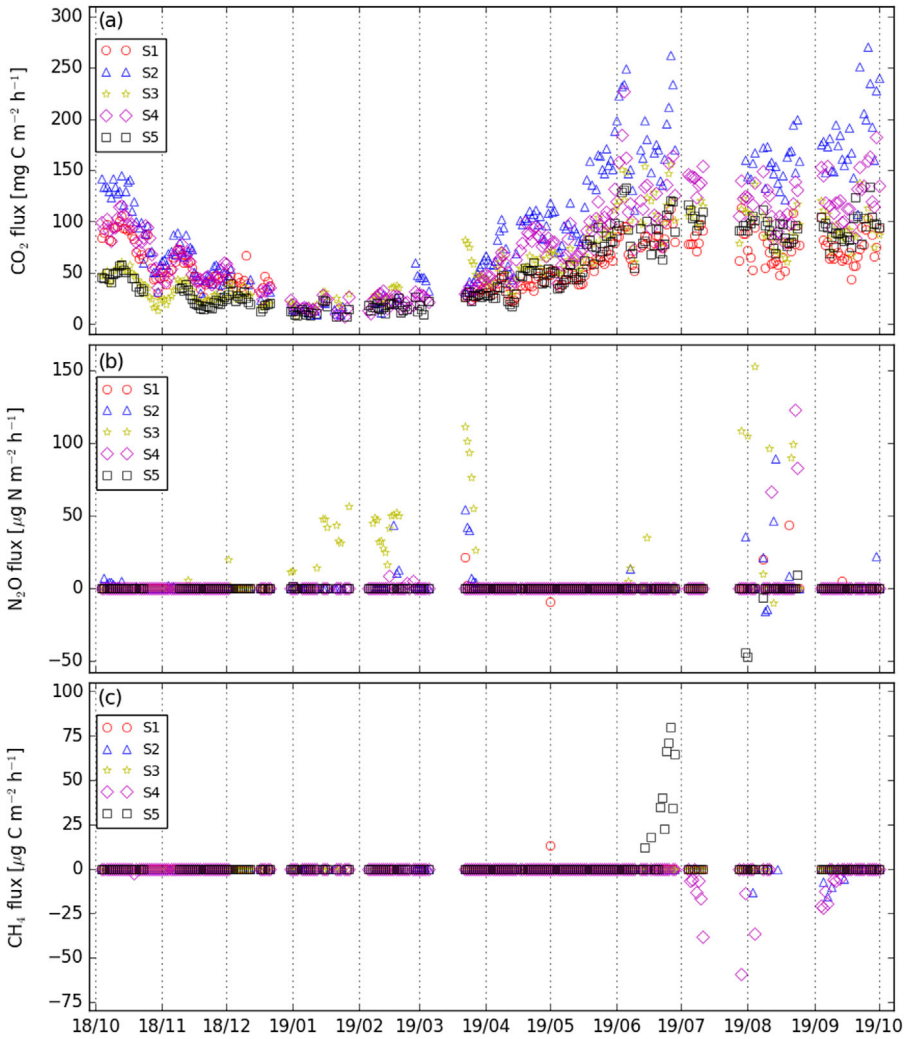

FIGURE 10 Variations in (a) CO_2 fluxes, (b) N_2O, and (c) CH_4 fluxes at S1 (Station 1), S2 (Station 2), S3 (Station 3), S4 (Station 4), and S5 (Station 5)

variable and the environmental factors as independent variables. The R^2 of the linear regression of CO_2 at the five stations ranged from .83 to .89, with soil temperature being the most important predictive variable (Supplemental Table S2). However, the stepwise approach leads to many similar regression coefficients (e.g., the WFPS having opposite signs at different levels). The stepwise regression results for N_2O and CH_4 were poor ($R^2 < .45$), indicating that CH_4 and N_2O are difficult to predict with simple linear regression models.

4 | DISCUSSION

4.1 | Eh monitoring

We found significant spatiotemporal differences in soil Eh indicated that the biogeochemical processes and their controls differed between the stations and even within the same soil horizons (Vereecken et al., 2016; Wanzek et al., 2018). These soil Eh variations in our studies are consistent with previous studies in that the mean Eh was lower for the soils that were more strongly influenced by groundwater, and Eh decreased with depth (Table 2 and Figure 5; Dwire et al., 2006; Mansfeldt, 2003; Yu et al., 2006), indicating limited O_2 diffusion during saturated conditions, which in turn triggered anoxic conditions (Ponnamperuma, 1972; Wang et al., 2018; Yang et al., 2006). Moreover, we found a distinct hysteresis in Eh changes after the groundwater table level changed during drying or rewetting phases. As in other studies, we found that the fluctuation of the groundwater level rapidly changed Eh, resulting in a more dynamic pattern (Seybold et al., 2002; Thomas et al., 2009). The large-scale pattern in the relationship between groundwater table and Eh is consistent: little variation in groundwater table depth resulted in relatively constant Eh (e.g. Station 1, Supplemental Figure S2), whereas increased variability in groundwater table resulted in stronger Eh variations. With the exception of Station 4, most redox sensors installed at 10-cm depth showed considerable higher Eh

values (around 600 mV) and only small variations after rainfall events occurred.

Even though the electrodes were below the water table level, the soil at −30-cm depths at Station 4 and 5 can exhibit higher Eh values after precipitation or water level increase, potentially due to the ability of wetland plants to transport O_2 from the atmosphere to the root zone (Grosse et al., 1992). Flessa and Fischer (1992) found that when soil is at reducing condition, the root zone of vegetation can even raise the Eh from the surface of the root from 120 to 420 mV.

The differences in soil wetness also affected revegetation of the deforested riparian zone: the further away from the stream, the more ryegrass (*Lolium perenne* L.) was growing, and the closer to the stream, the more bulrushes (*Juncus effusus* L.) were present. According to Shoemaker and Kröger (2017), the type of vegetation can also control the soil Eh dynamics. It should also be noted that the small-scale spatial variability may not have been adequately captured since we could only use two Eh sensors at each depth in our experiment. Other studies recommend the installation of 6 and up to 10 sensors per depth for soils with fluctuating groundwater levels (Fiedler et al., 2007; Wanzek et al., 2018).

4.2 | Soil respiration

In our study, we found that the average CO_2 emission in the riparian zone of the Wüstebach catchment was 71.58 ± 44.73 mg C m^{-2} h^{-1}, which is slightly below the mean values of other studies in temperate forests in Europe (75–79 mg C m^{-2} h^{-1}) (Rosenkranz et al., 2006; Wu et al., 2010). Ney et al. (2019) compared the CO_2 fluxes at the deforested and forested part at our research site, and the annual emission rate ranged from 91 to 96 mg C m^{-2} h^{-1}, which was slightly higher than in our riparian zone. Poblado et al. (2017) found higher CO_2 emission rates in a riparian zone in northeastern Spain (458 ± 308 mg C m^{-2} h^{-1} compared with 318 ± 195 mg C m^{-2} h^{-1}) in a subhumid Mediterranean climate. On the other hand, our CO_2 emission rates were significantly higher compared with a rehabilitated forest riparian zone in Ontario, Canada (27 ± 3 mg C m^{-2} h^{-1}), in a temperate climate with hot, humid summers and cold winters (De Carlo et al., 2019). The distances of their measurement chambers to the streams were within 32 m. Their experiments were performed in 2013 and from May 2015 to May 2016, respectively. Phillips and Nickerson (2015) and other studies (Fang & Moncrieff, 2001; Ludwig et al., 2001; Tang et al., 2003) assumed an exponential relationship between soil respiration and soil temperature. In accord with this assumption, the CO_2 flux has an exponential relationship with soil temperature in our study. Previous studies showed a distinct seasonal pattern of CO_2 fluxes, indicating the close relationship between CO_2 emissions and soil temperature (Kitzler et al., 2006; Papen & Butterbach-Bahl, 1999; Pilegaard et al., 2006; Schindlbacher et al., 2004; Suseela et al., 2012; Teiter & Mander, 2005; Wu et al., 2010). A correlation analysis revealed that soil respiration in the riparian zone was mainly dominated by soil temperature and WFPS due to lower microbial activity and limited O_2 availability (Monson et al., 2006). In the summer, the low soil moisture and high temperature were favorable for enhancing microbial activity and CO_2 emissions. However, in the colder and wetter seasons (winter and spring), they were unfavorable for the microbial activity (Mander et al., 2008). We found that CO_2 emission rates decreased with decreasing groundwater table depths (Supplemental Figure S7), suggesting that soil water is also an important controlling factor for CO_2 emission in the riparian zone as in other studies (Chang et al., 2014; Poblador et al., 2017). Station 1 showed the lowest CO_2 emissions during summer (July, August, and September) in 2019 due to dry soil conditions, as indicated by the low WFPS (28.1 ± 4.7%) values at −10 cm (Figure 10 and Supplemental Figure S2). Shi et al. (2014) found a positive correlation of CO_2 emissions with the C/N ratio. Therefore, the C/N ratio variations across the profiles at −10-cm soil layer may explain the higher annual CO_2 emission rate at Station 2 (C/N ratio = 19.7) than at Station 1 (C/N ratio = 12.8).

Marín-Muñiz et al. (2015) concluded that the Eh plays a vital role in GHG emissions in coastal wetlands. However, we found that the daily mean soil Eh had only a weak positive correlation with daily CO_2 emissions ($r = .21$) and similar to the results found by Gebremichael et al. (2017). Overall, regarding the relationship between the monthly average soil Eh at −30 cm and CO_2 fluxes, the soil Eh may help to interpret the dominant CO_2 flux from aerobic and anaerobic respiration, but this still needs to be investigated in further studies.

4.3 | Soil N_2O emissions and N variations

Because the Wüstebach catchment is an oligotrophic natural ecosystem, the soil N mainly originates from atmospheric dry and wet deposition, with some potential biological N fixation. Unlike fertilized agricultural soils, such soils are therefore unlikely to be a significant source of N_2O (Amundson & Davidson, 1990; Galloway et al., 2008). We found daily average N_2O emissions of 2.26 ± 12.72 μg N m^{-2} h^{-1}, which is similar to other studies in spruce forests (Krause et al., 2013; Wu et al., 2010) or riparian zones (Batson et al., 2015). Our results showed that the main N_2O emission occurred after heavy rainfall in winter followed by soil saturation, whereby denitrification can be assumed to be the main pathway due to the low soil Eh and high WFPS values at Station 3 (Pilegaard et al., 2006; Wolf & Russow, 2000 ; Yu et al., 2006). However, the N_2O emission occurred at Station 2 when the soil was in oxic condition at all depths (>+450 mV) during winter (Supplemental Figure S3), indicating that nitrification may have

been the dominant N_2O main pathway (Masscheleyn et al., 1993).

4.4 | CH_4 emissions

Compared with other studies in typical riparian zone wetlands, the CH_4 emission rates we found in the riparian zone of the Wüstebach catchment were very low. However, the study of Vidon et al. (2016) also showed uptake of CH_4 from only -20.41 ± 55.80 to -48.30 ± 6.25 μg C m^{-2} h^{-1} in a riparian zone that compares well to our results (Table 2). The main CH_4 production occurred at Station 5, and as Figure 6e shows, the CH_4 emission events started when soil Eh at −50 cm dropped below −150 mV, which has been described as a critical value for CH_4 production in soils (Wang et al., 1996; Yu & Patrick, 2003). However, higher threshold values have also been described in the literature, such as −110 mV for reed soils (Huang et al., 2001), or even as high as +300 mV, as found for a coastal forest at the Gulf of Mexico (Yu et al., 2006). In our study, conditions suitable for methanogenesis (high moisture and low soil Eh) mainly occurred in winter and spring, but the low temperatures during this period may be the reason for the low CH_4 production rate (Nazaries et al., 2013). Another explanation for the low observed CH_4 emission rates in our study could be that O_2–rich water of the lateral subsurface flow may have suppressed CH_4 production and emission in the riparian zone (Itoh et al., 2007). Although the soil Eh measured during CH_4 production at Station 5 was critical for CH_4 emissions at this station, we found that this particular Eh value was not suited to predict CH_4 emission at Station 3. Therefore, individual soil Eh measurements may be required in different soil types in order to obtain the specific critical soil Eh value for CH_4 production, especially in areas where soil properties, like in riparian zones, vary greatly at short distance. Stations 1, 2, and 3 showed hardly any CH_4 emission or uptake events, which is most likely due to the generally higher soil Eh values especially in the topsoil, which could intercept potential CH_4 production from deeper areas and thus preventing further emission to the atmosphere. Furthermore, the CH_4 emissions from Station 5 may have been enhanced by *Juncus effusus* L., allowing CH_4 to enter the roots in the highly reduced soil and bypass the methanotrophic layer at −10 cm (Henneberg et al, 2016). The low CH_4 emission and uptake rate indicated that our site was neither an important CH_4 sink nor source. Therefore, the CH_4 oxidation or emission represented only a small fraction of C cycling in this riparian zone.

5 | CONCLUSIONS

Here, we presented a newly developed automated measurement system for soil hydrological parameters and Eh in combination with GHG flux measurements, featuring real-time data transmission for better data management and maintenance. The observation system was deployed in a riparian zone of a deforested Norway spruce forest for 1 yr to trace the different microbial N_2O production pathways (nitrification or denitrification) and to characterize the dominant GHG. We found that mostly soil temperature as well as hydrologic events in the riparian zone controlled the GHG emissions. Most of the GHG emissions occurred in the form of CO_2 at our research site, even in the wet soils close to the stream. The daily mean soil–atmosphere exchange of CO_2 and N_2O at our site was $1{,}717.92 \pm 1{,}073.52$ mg CO_2–C m^{-2} d^{-1} and 54.24 ± 305.28 μg N m^{-2} d^{-1}. Soil temperature was identified as the most critical factor in controlling CO_2 emissions in our sites. We found that soil Eh in the surface soil layer showed hysteretic behavior in wetting and drying phases, and that soil Eh affected soil CO_2 emissions. In addition, by means of soil Eh measurements we were able to determine if the soil entered highly reduced conditions, which is the prerequisite for CH_4 production. Soil N_2O emissions varied across temporal and spatial scales, while both soil moisture and soil Eh helped to interpret soil N_2O sources and pathways. In summary, we could show that soil Eh measurements in riparian zones help to better understand the controls of GHG production. Therefore, we recommend implementing soil Eh measurements as routine components of long-term monitoring projects in critical zone observatories for better understanding the soil GHG production processes and their controlling factors.

ACKNOWLEDGMENTS

We gratefully acknowledge the support by the Chinese Scholarship Council (Scholarship no. 201506300053) and the TERENO project funded by the Helmholtz Association of German Research Centers. The authors also wish to thank Bernd Schilling, for his support during the experiments.

CONFLICT OF INTEREST

The authors declare no conflict of interest.

ORCID

Jihuan Wang https://orcid.org/0000-0002-0100-093X
Heye Bogena https://orcid.org/0000-0001-9974-6686
Thomas Süß https://orcid.org/0000-0002-9066-7065
Alexander Graf https://orcid.org/0000-0003-4870-7622
Nicolas Brüggemann https://orcid.org/0000-0003-3851-2418

REFERENCES

Adams, E. A. (2012). *World forest area still on the decline*. Earth Policy Institute. http://www.earth-policy.org/indicators/C56/forests_2012

Amundson, R. G., & Davidson, E. A. (1990). Carbon dioxide and nitrogenous gases in the soil atmosphere. *Journal of Geochemical*

Exploration, *38*, 13–41. https://doi.org/10.1016/0375-6742(90)90091-N

Batson, J., Noe, G. B., Hupp, C. R., Krauss, K. W., Rybicki, N. B., & Schenk, E. R. (2015). Soil greenhouse gas emissions and carbon budgeting in a short-hydroperiod floodplain wetland. *Journal of Geophysical Research: Biogeosciences*, *120*, 77–95. https://doi.org/10.1002/2014JG002817

Bogena, H. (2019). *Monitoring soil moisture pattern with wireless sensor networks: Technologies, applications and future perspectives*. University of Bonn.

Bogena, H. R., Huisman, J. A., Schilling, B., Weuthen, A., & Vereecken, H. (2017). Effective calibration of low-cost soil water content sensors. *Sensors*, *17*, 208. https://doi.org/10.3390/s17010208

Bogena, H. R., Montzka, C., Huisman, J. A., Graf, A., Schmidt, M., Stockinger, M., von Hebel, C., Hendricks-Franssen, H. J., van der Kruk, J., Tappe, W., Lücke, A., Baatz, R., Bol, R., Groh, J., Pütz, T., Jakobi, J., Kunkel, R., Sorg, J., & Vereecken, H. (2018). The TERENO-Rur hydrological observatory: A multiscale multi-compartment research platform for the advancement of hydrological science. *Vadose Zone Journal*, *17*, 180055. https://doi.org/10.2136/vzj2018.03.0055

Bohn, H. L. (1971). Redox potentials. *Soil Science*, *112*, 39–45. https://doi.org/10.1097/00010694-197107000-00007

Brettar, I., Sanchez-Perez, J. M., & Trémolieres, M. (2002). Nitrate elimination by denitrification in hardwood forest soils of the Upper Rhine floodplain-correlation with redox potential and organic matter. *Hydrobiologia*, *469*, 11–21. https://doi.org/10.1023/A:1015527611350

Brümmer, C., Brüggemann, N., Butterbach-Bahl, K., Falk, U., Szarzynski, J., Vielhauer, K., Wassmann, R., & Papen, H. (2008). Soil-atmosphere exchange of N_2O and NO in near-natural savanna and agricultural land in Burkina Faso (W. Africa). *Ecosystems*, *11*, 582–600. https://doi.org/10.1007/s10021-008-9144-1

Chang, C. T., Sabaté, S., Sperlich, D., Poblador, S., Sabater, F., & Gracia, C. (2014). Does soil moisture overrule temperature dependence of soil respiration in Mediterranean riparian forests?. *Biogeosciences*, *11*, 6173–6185. https://doi.org/10.5194/bg-11-6173-2014

Chapuis-Lardy, L., Wrage, N., Metay, A., Chotte, J. L., & Bernoux, M. (2007). Soils, a sink for N_2O? A review. *Global Change Biology*, *13*, 1–17. https://doi.org/10.1111/j.1365-2486.2006.01280.x

Clément, J. C., Pinay, G., & Marmonier, P. (2002). Seasonal dynamics of denitrification along topohydrosequences in three different riparian wetlands. *Journal of Environmental Quality*, *31*, 1025–1037. https://doi.org/10.2134/jeq2002.1025

Cogger, C. G., Kennedy, P. E., & Carlson, D. (1992). Seasonally saturated soils in the Puget Lowland II. Measuring and interpreting redox potentials. *Soil Science*, *154*, 50–58. https://doi.org/10.1097/00010694-199207000-00007

Collier, S. M., Ruark, M. D., Oates, L. G., Jokela, W. E., & Dell, C. J. (2014). Measurement of greenhouse gas flux from agricultural soils using static chambers. *Journal of Visualized Experiments*, *90*. https://doi.org/10.3791/52110

Comerford, N. B., Jerez, A., Freitas, A. A., & Montgomery, J. (1996). Soil water table, reducing conditions, and hydrologic regime in a Florida flatwood landscape. *Soil Science*, *161*, 194–199. https://doi.org/10.1097/00010694-199603000-00006

De Carlo, N. D., Oelbermann, M., & Gordon, A. M. (2019). Carbon dioxide emissions: Spatiotemporal variation in a young and mature riparian forest. *Ecological Engineering*, *138*, 353–361. https://doi.org/10.1016/j.ecoleng.2019.07.036

DeLaune, R. D., & Reddy, K. R. (2005). Redox potential. In *Encyclopedia of soils in the environment* (Vol. 3, pp. 366–371). Elsevier.

Durner, W., & Or, D. (2006). Soil water potential measurement. In M. G. Anderson & J. J. McDonnell (Eds.), *Encyclopedia of hydro-logical sciences* (pp. 1089–1102). John Wiley and Son. https://doi.org/10.1002/0470848944.hsa077a

Dutaur, L., & Verchot, L. V. (2007). A global inventory of the soil CH_4 sink. *Global Biogeochemical Cycles*, *21*. GB4013. https://doi.org/10.1029/2006GB002734

Dwire, K. A., Kauffman, J. B., & Baham, J. E. (2006). Plant species distribution in relation to water-table depth and soil redox potential in montane riparian meadows. *Wetlands*, *26*, 131–146. https://doi.org/10.1672/0277-5212(2006)26(131:PSDIRT)2.0.CO;2

Fang, C., & Moncrieff, J. (2001). The dependence of soil CO_2 efflux on temperature. *Soil Biology and Biochemistry*, *33*, 155–165. https://doi.org/10.1016/S0038-0717(00)00125-5

Fiedler, S., Vepraskas, M. J., & Richardson, J. L. (2007). Soil redox potential: Importance, field measurements, and observations. *Advances in Agronomy*, *94*, 1–54. https://doi.org/10.1016/S0065-2113(06)94001-2

Flessa, H., & Fischer, W. R. (1992). Plant-induced changes in the redox potentials of rice rhizospheres. *Plant and Soil*, *143*, 55–60. https://doi.org/10.1007/BF00009128

Galloway, J. N., Townsend, A. R., Erisman, J. W., Bekunda, M., Cai, Z., Freney, J. R., Martinelli, L. A., Seitzinger, S. P., & Sutton, M. A. (2008). Transformation of the nitrogen cycle: Recent trends, questions, and potential solutions. *Science*, *320*, 889–892. https://doi.org/10.1126/science.1136674

Gebremichael, A. W., Osborne, B., & Orr, P. (2017). Flooding-related increases in CO_2 and N_2O emissions from a temperate coastal grassland ecosystem. *Biogeosciences*, *14*, 2611–2626. https://doi.org/10.5194/bg-14-2611-2017

Grosse, W., Frye, J., & Lattermann, S. (1992). Root aeration in wetland trees by pressurized gas transport. *Tree Physiology*, *10*, 285–295. https://doi.org/10.1093/treephys/10.3.285

Henneberg, A., Brix, H., & Sorrell, B. K. (2016). The interactive effect of *Juncus effusus* and water table position on mesocosm methanogenesis and methane emissions. *Plant and Soil*, *400*, 45–54. https://doi.org/10.1007/s11104-015-2707-y

Huang, G., Li, Y., Chen, G., Yang, Y., & Zhao, C. (2001). Influence of environmental factors on CH_4 emission from reed wetland. *Huanjing Kexue*, *22*, 1–5.

Husson, O. (2013). Redox potential (Eh) and pH as drivers of soil/plant/microorganism systems: A transdisciplinary overview pointing to integrative opportunities for agronomy. *Plant and Soil*, *362*, 389–417. https://doi.org/10.1007/s11104-012-1429-7

Husson, O., Husson, B., Brunet, A., Babre, D., Alary, K., Sarthou, J. P., Hubert, C., Michel, D., Jaroslav, B., & Henry, M. (2016). Practical improvements in soil redox potential (Eh) measurement for characterisation of soil properties. Application for comparison of conventional and conservation agriculture cropping systems. *Analytica Chimica Acta*, *906*, 98–109. https://doi.org/10.1016/j.aca.2015.11.052

Itoh, M., Ohte, N., Koba, K., Katsuyama, M., Hayamizu, K., & Tani, M. (2007). Hydrologic effects on methane dynamics in riparian wetlands in a temperate forest catchment. *Journal of Geophysical Research: Biogeosciences*, *112*. https://doi.org/10.1029/2006JG000240

Kitzler, B., Zechmeister-Boltenstern, S., Holtermann, C., Skiba, U., & Butterbach-Bahl, K. (2006). Controls over N_2O, NO_x and CO_2 fluxes in a calcareous mountain forest soil. *Biogeosciences*, *3*, 383–395. https://doi.org/10.5194/bg-3-383-2006

Krause, K., Niklaus, P. A., & Schleppi, P. (2013). Soil-atmosphere fluxes of the greenhouse gases CO_2, CH_4 and N_2O in a mountain spruce forest subjected to long-term N addition and to tree girdling. *Agricultural and Forest Meteorology*, *181*, 61–68. https://doi.org/10.1016/j.agrformet.2013.07.007

Ludwig, J., Meixner, F. X., Vogel, B., & Förstner, J. (2001). Soil-air exchange of nitric oxide: An overview of processes, environmental factors and modeling studies. *Biogeochemistry*, *52*, 225–257. https://doi.org/10.1023/A:1006424330555

Mander, Ü., Lohmus, K., Teiter, S., Uri, V., & Augustin, J. (2008). Gaseous nitrogen and carbon fluxes in riparian alder stands. *Boreal Environment Research*, *13*, 231–241. http://hdl.handle.net/10138/234735

Mansfeldt, T. (2003). In situ long-term redox potential measurements in a dyked marsh soil. *Journal of Plant Nutrition and Soil Science*, *166*, 210–219. https://doi.org/10.1002/jpln.200390031

Mansfeldt, T. (2004). Redox potential of bulk soil and soil solution concentration of nitrate, manganese, iron, and sulfate in two Gleysols. *Journal of Plant Nutrition and Soil Science*, *167*, 7–16. https://doi.org/10.1002/jpln.200321204

Marín-Muñiz, J. L., Hernández, M. E., & Moreno-Casasola, P. (2015). Greenhouse gas emissions from coastal freshwater wetlands in Veracruz Mexico: Effect of plant community and seasonal dynamics. *Atmospheric Environment*, *107*, 107–117. https://doi.org/10.1016/j.atmosenv.2015.02.036

Masscheleyn, P. H., DeLaune, R. D., & Patrick Jr, W. H. (1993). Methane and nitrous oxide emissions from laboratory measurements of rice soil suspension: Effect of soil oxidation-reduction status. *Chemosphere*, *26*, 251–260. https://doi.org/10.1016/0045-6535(93)90426-6

McDaniel, P. A., Gabehart, R. W., Falen, A. L., Hammel, J. E., & Reuter, R. J. (2001). Perched water tables on Argixeroll and Fragixeralf hillslopes. *Soil Science Society of America Journal*, *65*, 805–810. https://doi.org/10.2136/sssaj2001.653805x

Monson, R. K., Lipson, D. L., Burns, S. P., Turnipseed, A. A., Delany, A. C., Williams, M. W., & Schmidt, S. K. (2006). Winter forest soils respiration controlled by climate and microbial community composition. *Nature*, *439*, 711–714. https://doi.org/10.1038/nature04555

Nazaries, L., Murrell, J. C., Millard, P., Baggs, L., & Singh, B. K. (2013). Methane, microbes and models: Fundamental understanding of the soil methane cycle for future predictions. *Environmental Microbiology*, *15*, 2395–2417. https://doi.org/10.1111/1462-2920.12149

Ney, P., Graf, A., Bogena, H., Diekkrüger, B., Drüe, C., Esser, O., Heinemann, G., Klosterhalfen, A., Pick, K., Pütz, T., Schmidt, M., Valler, V., & Vereecken, H. (2019). CO_2 fluxes before and after partial deforestation of a Central European spruce forest. *Agricultural and Forest Meteorology*, *274*, 61–74. https://doi.org/10.1016/j.agrformet.2019.04.009

Oertel, C., Matschullat, J., Zurba, K., Zimmermann, F., & Erasmi, S. (2016). Greenhouse gas emissions from soils-A review. *Geochemistry*, *76*, 327–352. https://doi.org/10.1016/j.chemer.2016.04.002

Papen, H., & Butterbach-Bahl, K. (1999). A 3-year continuous record of nitrogen trace gas fluxes from untreated and limed soil of a N-saturated spruce and beech forest ecosystem in Germany: 1. N_2O emissions. *Journal of Geophysical Research: Atmospheres*, *104*, 18487–18503. https://doi.org/10.1029/1999JD900293

Parkin, T. B., & Venterea, R. T. (2010). USDA-ARS GRACEnet project protocols: Chamber-based trace gas flux measurements. In R. F. Follett (Ed.), *Sampling protocols* (pp. 3-1–3-39). USDA-ARS.

Patrick, W. H., & Jugsujinda, A. (1992). Sequential reduction and oxidation of inorganic nitrogen, manganese, and iron in flooded soil. *Soil Science Society of America Journal*, *56*, 1071–1073. https://doi.org/10.2136/sssaj1992.03615995005600040011x

Phillips, C. L., & Nickerson, N. (2015). Soil respiration. In *Reference module in earth systems and environmental sciences*. Elsevier. https://doi.org/10.1016/B978-0-12-409548-9.09442-2

Phillips, R., & Beeri, O. (2008). The role of hydropedologic vegetation zones in greenhouse gas emissions for agricultural wetland landscapes. *Catena*, *72*, 386–394. https://doi.org/10.1016/j.catena.2007.07.007

Pilegaard, K., Skiba, U., Ambus, P., Beier, C., Bruggemann, N., Butterbach-Bahl, K., Dick, J., Dorsey, J., Duyzer, J., Gallagher, M., Gasche, R., Horvath, L., Kitzler, B., Leip, A., Pihlatie, M. K., Rosenkranz, P., Seufert, G., Vesala, T., Westrate, H., & Zechmeister-Boltenstern, S. (2006). Factors controlling regional differences in forest soil emission of nitrogen oxides (NO and N_2O). *Biogeosciences*, *3*, 651–661. https://doi.org/10.5194/bg-3-651-2006

Poblador, S., Lupon, A., Sabaté, S., & Sabater, F. (2017). Soil water content drives spatiotemporal patterns of CO_2 and N_2O emissions from a Mediterranean riparian forest soil. *Biogeosciences*, *14*, 4195–4208. https://doi.org/10.5194/bg-14-4195-2017

Ponnamperuma, F. N. (1972). The chemistry of submerged soils. *Advances in Agronomy*, *24*, 29–96. https://doi.org/10.1016/S0065-2113(08)60633-1

Reddy, K. R., Patrick Jr, W. H., & Lindau, C. W. (1989). Nitrification-denitrification at the plant root-sediment interface in wetlands. *Limnology and Oceanography*, *34*, 1004–1013. https://doi.org/10.4319/lo.1989.34.6.1004

Rinklebe, J., Shaheen, S. M., & Frohne, T. (2016). Amendment of biochar reduces the release of toxic elements under dynamic redox conditions in a contaminated floodplain soil. *Chemosphere*, *142*, 41–47. https://doi.org/10.1016/j.chemosphere.2015.03.067

Rosenkranz, P., Bruggemann, N., Papen, H., Xu, Z., Seufert, G., & Butterbach-Bahl, K. (2006). N_2O, NO and CH_4 exchange, and microbial N turnover over a Mediterranean pine forest soil. *Biogeosciences*, *3*, 121–133. https://doi.org/10.5194/bg-3-121-2006

Schindlbacher, A., Zechmeister-Boltenstern, S., & Butterbach-Bahl, K. (2004). Effects of soil moisture and temperature on NO, NO_2, and N_2O emissions from European forest soils. *Journal of Geophysical Research: Atmospheres*, *109*. https://doi.org/10.1029/2004JD004590

Seybold, C. A., Mersie, W., Huang, J., & McNamee, C. (2002). Soil redox, pH, temperature, and water-table patterns of a freshwater tidal wetland. *Wetlands*, *22*, 149–158 https://doi.org/10.1672/0277-5212(2002)022(0149:SRPTAW)2.0.CO;2

Shi, W. Y., Yan, M. J., Zhang, J. G., Guan, J. H., & Du, S. (2014). Soil CO_2 emissions from five different types of land use on the semiarid Loess Plateau of China, with emphasis on the contribution of winter soil respiration. *Atmospheric Environment*, *88*, 74–82. https://doi.org/10.1016/j.atmosenv.2014.01.066

Shoemaker, C., & Kröger, R. (2017). Frequentist and Bayesian approaches to understanding changes in redox potential due to hydrology and vegetation in agricultural drainage ditches. *Wetlands*, *37*, 705–714. https://doi.org/10.1007/s13157-017-0901-9

Smith, C. J., & DeLaune, R. D. (1984). Effect of rice plants on nitrification-denitrification loss of nitrogen under greenhouse

conditions. *Plant and Soil*, *79*, 287–290. https://doi.org/10.1007/BF02182351

Smith, P., Martino, D., Cai, Z., Gwary, D., Janzen, H., Kumar, P., McCarl, B., Ogle, S., O'Mara, F., Rice, C., Scholes, B., & Sirotenko, O. (2007). *Climate change 2007: Mitigation of climate change: Working Group III contribution to the Fourth Assessment Report of the IPCC*. Cambridge University Press. https://doi.org/10.1017/CBO9780511546013

Suseela, V., Conant, R. T., Wallenstein, M. D., & Dukes, J. S. (2012). Effects of soil moisture on the temperature sensitivity of heterotrophic respiration vary seasonally in an old-field climate change experiment. *Global Change Biology*, *18*, 336–348. https://doi.org/10.1111/j.1365-2486.2011.02516.x

Tang, J., Baldocchi, D. D., Qi, Y., & Xu, L. (2003). Assessing soil CO_2 efflux using continuous measurements of CO_2 profiles in soils with small solid-state sensors. *Agricultural and Forest Meteorology*, *118*, 207–220. https://doi.org/10.1016/S0168-1923(03)00112-6

Teiter, S., & Mander, Ü. (2005). Emission of N_2O, N_2, CH_4, and CO_2 from constructed wetlands for wastewater treatment and from riparian buffer zones. *Ecological Engineering*, *25*, 528–541. https://doi.org/10.1016/j.ecoleng.2005.07.011

Thomas, C. R., Miao, S., & Sindhoj, E. (2009). Environmental factors affecting temporal and spatial patterns of soil redox potential in Florida Everglades wetlands. *Wetlands*, *29*, 1133–1145. https://doi.org/10.1672/08-234.1

Tokarz, E., & Urban, D. (2015). Soil redox potential and its impact on microorganisms and plants of wetlands. *Journal of Ecological Engineering*, *16*, 20–30. https://doi.org/10.12911/22998993/2801

Vepraskas, M. J., & Wilding, L. P. (1983). Albic Neoskeletans in Argillic Horizons as indices of seasonal saturation and iron reduction. *Soil Science Society of America Journal*, *47*, 1202–1208. https://doi.org/10.2136/sssaj1983.03615995004700060028x

Vereecken, H., Schnepf, A., Hopmans, J. W., Javaux, M., Or, D., Roose, T., Vanderborght, J., Young, M. H., Amelung, W., Aitkenhead, M., Allison, S. D., Assouline, S., Baveye, P., Berli, M., Brüggemann, N., Finke, P., Flury, M., Gaiser, T., Govers, G., . . . , & Young, I. M. (2016). Modeling soil processes: Review, key challenges, and new perspectives. *Vadose Zone Journal*, *15*. https://doi.org/10.2136/vzj2015.09.0131

Vidon, P., Marchese, S., Welsh, M., & McMillan, S. (2016). Impact of precipitation intensity and riparian geomorphic characteristics on greenhouse gas emissions at the soil-atmosphere interface in a water-limited riparian zone. *Water, Air, and Soil Pollution*, *227*, 8. https://doi.org/10.1007/s11270-015-2717-7

Wagner, K. (2019). *Impact assessment of land-use change and agricultural treatments on greenhouse gas emissions from wetlands of Uganda and Tanzania* (Doctoral dissertation, Rheinische Friedrich-Wilhelms-Universität Bonn).

Wang, J., Bogena, H. R., Vereecken, H., & Brüggemann, N. (2018). Characterizing redox potential effects on greenhouse gas emissions induced by water-level changes. *Vadose Zone Journal*, *17*. https://doi.org/10.2136/vzj2017.08.0152

Wang, J., Bogena, H. R., Vereecken, H., & Brüggemann, N. (2020). Stable-isotope-aided investigation of the effect of redox potential on nitrous oxide emissions as affected by water status and N fertilization. *Water*, *12*, 2918. https://doi.org/10.3390/w12102918

Wang, Z., Zeng, D., & Patrick, W. H. (1996). Methane emissions from natural wetlands. *Environmental Monitoring and Assessment*, *42*, 143–161. https://doi.org/10.1029/GB001i001p00061

Wanzek, T., Keiluweit, M., Baham, J., Dragila, M. I., Fendorf, S., Fiedler, S., Nico, P. S., & Kleber, M. (2018). Quantifying biogeochemical heterogeneity in soil systems. *Geoderma*, *324*, 89–97. https://doi.org/10.1016/j.geoderma.2018.03.003

Wiekenkamp, I., Huisman, J. A., Bogena, H. R., Graf, A., Lin, H. S., Drüe, C., & Vereecken, H. (2016). Changes in measured spatiotemporal patterns of hydrological response after partial deforestation in a headwater catchment. *Journal of Hydrology*, *542*, 648–661. https://doi.org/10.1016/j.jhydrol.2016.09.037

Wolf, I., & Russow, R. (2000). Different pathways of formation of N_2O, N_2 and NO in black earth soil. *Soil Biology & Biochemistry*, *32*, 229–239. https://doi.org/10.1016/S0038-0717(99)00151-0

Wu, X., Brüggemann, N., Gasche, R., Shen, Z., Wolf, B., & Butterbach-Bahl, K. (2010). Environmental controls over soil-atmosphere exchange of N_2O, NO, and CO_2 in a temperate Norway spruce forest. *Global Biogeochemical Cycles*, *24*. https://doi.org/10.1029/2009GB003616

Yang, J., Hu, Y., & Bu, R. (2006). Microscale spatial variability of redox potential in surface soil. *Soil Science*, *171*, 747–753. https://doi.org/10.1097/01.ss.0000230127.86394.45

Yu, K., Chen, G., & Patrick, W. H. Jr. (2004). Reduction of global warming potential contribution from a rice field by irrigation, organic matter, and fertilizer management. *Global Biogeochemical Cycles*, *18*. https://doi.org/10.2136/sssaj2003.1952

Yu, K., Faulkner, S. P., & Baldwin, M. J. (2008). Effect of hydrological conditions on nitrous oxide, methane, and carbon dioxide dynamics in a bottomland hardwood forest and its implication for soil carbon sequestration. *Global Change Biology*, *14*, 798–812. https://doi.org/10.1111/j.1365-2486.2008.01545.x

Yu, K., Faulkner, S. P., & Patrick, W. H. Jr. (2006). Redox potential characterization and soil greenhouse gas concentration across a hydrological gradient in a Gulf Coast forest. *Chemosphere*, *62*, 905–914. https://doi.org/10.1016/j.chemosphere.2005.05.033

Yu, K., & Patrick, W. H. (2003). Redox range with minimum nitrous oxide and methane production in a rice soil under different pH. *Soil Science Society of America Journal*, *67*, 1952–1958. https://doi.org/10.2136/sssaj2003.1952

SUPPORTING INFORMATION

Additional supporting information may be found online in the Supporting Information section at the end of the article.

How to cite this article: Wang, J, Bogena, H, Süß, T, Graf, A, Weuthen, A, & Brüggemann, N Investigating the controls on greenhouse gas emission in the riparian zone of a small headwater catchment using an automated monitoring system. *Vadose Zone J.* 2021;*20:*e20149. https://doi.org/10.1002/vzj2.20149